Inflammation, Vol. 42, No. 2, April 2019 (© 2018)
DOI: 10.1007/s10753-018-0932-2

ORIGINAL ARTICLE

Metabolomics Analysis Reveals Therapeutic Effects of α-Mangostin on Collagen-Induced Arthritis in Rats by Down-regulating Nicotinamide Phosphoribosyltransferase

Kui Yang,[1] Qin Yin,[2] Qingcheng Mao,[3] Sheng Dai,[4] Lin Wang,[1] Jiyang Dong,[5] and Jian Zuo[1,6]

Abstract—α-Mangostin (MAN) is a bioactive compound isolated from pericarp of mangosteen (*Garcinia mangostana* Linn.) with significant anti-rheumatic potentials. The purpose of this study was to explore the mechanisms underlying its therapeutic effects on collagen-induced arthritis (CIA) in rats with metabolomics approaches. Therapeutic effects of MAN on CIA were assessed by radiographic, histological, and immunohistochemical methods. Metabolic profiles of rats were characterized based on UPLC-MS/MS analysis of urine samples, followed by verification in HFLS-RA cells using a variety of toxicological and biochemical assays. We found that MAN treatment protected joint structures in CIA rats and caused a decrease of nicotinamide mononucleotide (NMN) in urine. The levels of nicotinamide phosphoribosyltransferase (NAMPT) were reduced in fibroblast-like synoviocytes by MAN both *in vivo* and *in vitro*, which was accompanied with a decline in nicotinamide adenine dinucleotide (NAD) production. Secretion of extracellular NAMPT (eNAMPT) in HFLS-RA cells was also decreased upon MAN treatment, which lagged behind the changes of its intracellular counterpart (iNAMPT). Co-treatment with NMN raised the secretion of eNAMPT and restored the decline of p-p65 and TNF-α induced by MAN *in vitro*. Sirt1 expression was down-regulated under MAN treatments too. These results suggest that MAN treatment suppressed NAD production by inhibiting iNAMPT expression, which in turn decreased eNAMPT secretion and alleviated NF-κB-mediated inflammations in CIA rats.

KEY WORDS: xanthone; rheumatoid arthritis; NAD; metabolism; inflammation.

Kui Yang and Qin Yin contributed equally to this work.

Electronic supplementary material The online version of this article (https://doi.org/10.1007/s10753-018-0932-2) contains supplementary material, which is available to authorized users.

[1] Yijishan Hospital of Wannan Medical College, 2 West Zheshan Road, Wuhu, 241000, China
[2] The Second Affiliated Hospital of Wannan Medical College, Wuhu, 241000, China
[3] Department of Pharmaceutics, School of Pharmacy, University of Washington, Seattle, WA 98195, USA
[4] Anhui College of Traditional Chinese Medicine, Wuhu, 241000, China
[5] Department of Electronic Science, Xiamen University, Xiamen, 361005, China
[6] To whom correspondence should be addressed at Yijishan Hospital of Wannan Medical College, 2 West Zheshan Road, Wuhu, 241000, China. E-mail: zuojian8178@163.com

INTRODUCTION

We previously conducted a systematic chemical isolation of a traditional anti-rheumatic herbal medicine and obtained a series of xanthone derivatives [1], which have been subsequently validated with significant therapeutic potentials against experimental arthritis through targeting specific pro-inflammatory pathways in fibroblast-like synoviocyte (FLS) [2, 3]. However, the simple oxygenated substituent groups of these xanthones determine the planar-like structures and low aqueous solubility, which eventually lead to the poor bioavailability. To achieve better therapeutic effects, we have been actively screening more effective agents from their analogues.

The inedible pericarp of mangosteen (*Garcinia mangostana* Linn.) is used as a medicine to cure inflammatory diseases in Southern Asia traditionally. It is abundant with α-mangostin (MAN), a prenylated xanthone derivative [4]. We found that MAN possessed a stronger anti-rheumatic potential on adjuvant-induced arthritis (AA) in rats than previously investigated counterparts [5]. Additionally, MAN abundant mangosteen extract significantly restored the immune homeostasis and protected joints from destruction in collagen-induced arthritis (CIA) rats [6]. Given its high abundance in nature and high safety profile, the application of MAN in rheumatoid arthritis (RA) therapies appears to be promising. Although we have revealed that down-regulation of NF-κB is responsible for the therapeutic effects of MAN on experimental arthritis [5], exact molecular targets contributing to this critical signaling change have not been identified.

To further elucidate the mechanisms and identify the molecular targets of MAN in treating RA, in this study, we performed an UPLC-MS/MS-based metabolomics analysis with urine samples collected from CIA rats receiving MAN treatment. The results obtained were further validated by *in vitro* toxicological and biological experiments.

MATERIALS AND METHODS

Chemicals and Reagents

MAN with the purity of 98% and biological reagent grade 2-chloro-L-phenylalanine were purchased from SanHerb Bioscience Inc. (Chengdu, Sichuan, China) and HengBai Biotechnology (Shanghai, China), respectively. Immunization grade incomplete Freund's adjuvant (IFA) and lyophilized bovine type II collagen (CII) were obtained from Chondex Inc. (Redmond, WA, USA). Nicotinamide adenine dinucleotide (NAD), nicotinamide mononucleotide (NMN), MTT, PBS, DMSO, LPS, BCA quantitative kit, HRP-conjugated streptavidin, and HRP/biotin conjugated secondary antibodies were from KeyGen Biotech (Nanjing, Jiangsu, China). Fetal bovine serum (FBS), high glucose DMEM, ECL detection kit, defatted milk powder, and bovine serum albumin (BSA) were purchased from Thermo Scientific (Rockford, IL, USA). All primary antibodies were products of Affinity Biosciences (Cincinnati, OH, USA). Ultra-pure water was obtained from a Milli-Q purification system (Millipore, Bedford, MA, USA). Other solvents of chromatographic grade were supplied by Merck Chemicals (Shanghai, China).

Induction of CIA in Rats and Treatments

IFA and CII solutions (2 mg/ml in 0.05 M acetic acid) were mixed equally in an ice-water bath to obtain a milky homogeneous emulsion that was used to induce CIA in male SD rats (7 weeks old) *via* a multiple-point subcutaneous injection in the back and base of the tail. The induced rats were then divided into two groups (six rats each) that served as the CIA control and MAN treatment group, respectively. Another six healthy rats were adopted as normal controls. Afterwards, the rats received different treatments for 45 days. Rats in MAN group were given MAN suspension (in CMC-Na solution) by oral gavage at the dose of 40 mg/kg daily. CIA models and normal controls were treated with 0.5% CMC-Na synchronously.

Sampling and Radiological Assessment

Two days ahead of sacrifice, all rats were kept in separate metabolism cages for 24 h individually, and the total urine from each rat was collected through automatic micturition. After a high speed centrifugation at 4 °C, the supernatant was collected, divided into aliquots, and stored at − 80 °C until analysis.

By the end of treatments, all the rats were anesthetized with 10% chloral hydrate solution, and the severity of joints destruction was assessed with a radiological examination. Then, the animals were sacrificed. The hind limbs including ankle joints were promptly dissected from the body and fixed in 10% neutral buffered formalin.

Histological and Immunohistochemical Examinations

The fixed joints were decalcified with 10% EDTA for 2 weeks and embedded in paraffin. The blocks were cut into sections at a thickness of 4 μm, which were then mounted on glass slides. Subsequently, processed specimens were stained with hematoxylin and eosin, and observed by the aid of an Olympus BH-2 light microscope (Tokyo, Japan). The severity of CIA was evaluated based on bone/cartilage destruction, synovial hyperplasia, and inflammatory infiltration in joints.

To perform immunohistochemical examinations, certain sections were deparaffinized with xylene and rehydrated in PBS. Endogenous peroxidases were deactivated by 3% hydrogen peroxide, and the antigen retrieval was achieved by citric acid treatment coupled with microwave heating. After being blocked with normal goat serum, the sections were incubated with the anti-NAMPT or Sirt1 rabbit polyclonal antibody (dilution ratio of 1:100) at 4 °C overnight. After three washes with PBS, the slides

were treated with goat anti-rabbit biotin-labeled secondary antibody (dilution ratio of 1:2000) at room temperature followed by the incubation with HRP-conjugated streptavidin. Finally, the specific proteins were visualized by diaminobenzidine staining, and another counterstained staining with hematoxylin was also carried out.

Urine Sample Preparation

One hundred microliters of urine sample together with 20 μl of L-2-chlorophenylalanineas stock (1 mg/ml in water, served as internal standard) were spiked into 900 μl of the extraction solvent (methanol-acetonitrile-water, 2:2:1). The mixture was thoroughly mixed and kept at − 20 °C for 1 h. After a high speed centrifugation, 700 μl of the supernatant was obtained and dried in a vacuum centrifugal concentrator (Eppen-dorf AG, Hamburg, Germany) without heating. The analyte was reconstituted with 300 μl of acetonitrile-water (1:1), and further centrifuged at 12000 rpm for 15 min. The supernatant was then collected and injected into UPLC-QTOF-MS for analysis. Some additional samples within the same group were mixed equally to prepare the pooled quality control (QC).

UPLC-MS/MS Analysis

Chromatographic separation of the analytes was performed on an ACQUITY UPLC HSS T3 column (100 × 2.1 mm, 1.7 μm, Waters, Milford, MA, USA) using a 1290 infinity UPLC system (Agilent Technologies, Santa Clara, CA, US). The column temperature was set at 25 °C, and a gradient elution method at the flow rate of 0.5 ml/min was employed. Ammonium acetate/ammonium hydroxide buffer (25 mM) and acetonitrile were used as mobile phases A and B, respectively. The elution gradient was as follows: 90% B (0–0.5 min), 90–40% B (0.5–8 min), 40–95% B (8-12 min), and 95% B (12–14 min).

Mass spectrometry was performed on an Agilent 6550 iFunnel Q-TOF system (Agilent Technologies, Santa Clara, CA, US) coupled with an electrospray ionization source interface operating at both positive and negative ion modes. Main parameters were summarized as follows: drying gas temperature, 250 °C; drying gas flow, 16 L/min; nebulizer, 20 psig; sheath gas temperature, 400 °C; sheath gas flow, 12 L/min; capillary voltage, 3000 V; fragmentor, 175 V; mass range (*m*/*z*), 50–1200; acquisition rate, 4 Hz; cycle time, 250 ms. At intervals of every four tests, QC samples were analyzed to monitor the stability of the analysis method.

Metabolite Identification and Data Analysis

Signals in raw data acquired from UPLC-MS/MS procedures were calibrated with the internal standard and processed with an online statistical R package XCMS to filter noise, simulate missing value, match common peaks, and sequence retention time. The peaks varying within the range of *m*/*z* tolerance 30 ppm and retention time tolerance 20 s were accepted as identical. To reduce redundant signals, peaks with intensity RSD over 30% in pooled QC set were removed. Afterwards, the data was normalized based on the peak intensities sum. By searching a commercial metabolomics library constructed by Biotree Biotech on the same experimental platform with purified standards, metabolites were identified by retention time, *m*/*z* and MS^2 characteristics. To overview the general differences among groups, we performed an initial exploratory principal component analysis (PCA) using the SIMCA-P V14.1 program (Umetrics, Umea, Sweden). A seven-fold cross-validated orthogonal partial least squares discriminate analysis (OPLS-DA) model was employed to further explore differences among groups. The discriminatory metabolites (variable importance in the projection, VIP > 1) with statistical significance $p < 0.05$ (based on two-tails Student's *t* test) were visualized in the heat-map and applied in the pathway enrichment analysis and KEGG annotation.

NAD Determination

Twenty-four male SD rats were assigned into four groups randomly. Three groups received intragastrical MAN at different doses for 3 consecutive days (10, 20, and 40 mg/kg/day). Another group received CMC-Na instead. Three hours after the last administration, blood from each rat was collected for serum separation by the means of centrifugation at 3000 rpm for 10 min after coagulation. NAD^+ in serum was determined using a NAD quantification kit (Solarbio Science & Technology Co., Ltd., Beijing, China) according to the manufacturer's protocol.

A FLS-derived cell line HFLS-RA (Jennio Biotech, Guangzhou, China) was used in *in vitro* experiments. The cells were grown in high glucose DMEM supplemented with 10% FBS and penicillin-streptomycin (100 U/ml) in a humidified 37 °C, 5% CO_2 incubator. The passage of cells was carried out every 2–3 days at the ratio of 1:3. To determine intracellular NAD^+ and NADH concentrations, cells were seeded into 75 cm^2 culture flasks and treated with MAN at different concentrations (0, 8, 10, and 12 μg/ml) for 6 or 24 h. Then, cells were harvested and

counted. Three to six million cells were lysed in 500 μl of extraction solution provided in the quantitative assay kit. The resulting cell lysates were denatured in boiling water bath and centrifuged at 12000 rpm for 10 min at 4 °C. The supernatant was collected for NAD^+/NADH concentration determination by using the same kit mentioned above. The relative intracellular NAD^+/NADH levels were calculated based on the quantified concentrations normalized to cell counts.

MTT and ROS Assays

In the MTT assay, cells were seeded into 96-well plates at the density of 1×10^4 per well. After an overnight incubation, MAN at various concentrations with or without NMN/NAD (200 μM) was added in triplicate. By the end of treatments, 20 μl of MTT solution (5 mg/ml in PBS) was added, followed by a further incubation at 37 °C for 4 h. DMSO was used to dissolve formazan, and the optical density was measured by a microplate spectrophotometer (BIO-RAD Science Co. Ltd., USA) at 490 nm.

The fluorescent probe DCFH-DA (Beyotime Biotech, Nantong, China) was used to evaluate the intracellular oxidative stress according to the manufacture's protocol. Briefly, HFLS-RA cells were incubated with MAN at 12 μg/ml for pre-determined times (0, 6, 12, or 24 h) after attachment. Then, the medium was replaced by FBS free/DCFH-DA containing DMEM (10 μM). A further incubation at 37 °C for 20 min in dark was carried out to allow DCFH-DA to permeate into cells. Thereafter, the cells were washed two times with ice-cold PBS to remove excessive probe. As excitation and emission wavelengths for DCFH-DA are 488 and 530 nm respectively, we observed and recorded the green fluorescence under the blue light irradiation using an Olympus BX53 fluorescence microscope (Tokyo, Japan).

Immunoblotting and ELISA Analysis

Prior to the assays, cells were seeded into 6-well plates at the density of 1×10^5 per well. Then, attached cells were treated with MAN in the absence or presence of NMN/NAD (200 μM) for certain times (3, 6, or 24 h), and some of the cells were pre-treated with LPS at 10 ng/ml to mimic the inflammatory conditions *in vivo*. The supernatants from culture media were collected for ELISA assays strictly in accordance with the manufacturer's instructions, while the cells were lysed with cold RIPA buffer for immunoblotting. After a centrifugation at 12000 rpm for 15 min at 4 °C, the supernatants of cell lysates were collected. Protein concentrations in them were quantified by using a BCA kit, and the supernatants were spiked into loading buffer and denatured by boiling. Samples containing equal amount of proteins (20 μg) were subject to SDS-PAGE. The separated proteins were then transferred onto nitrocellulose membranes that were blocked with 5% defatted milk and treated by primary and HRP-conjugated secondary antibodies in turns. After extensive washing, signals were detected using an ECL kit on a Tanon 5200 system (Bio-Tanon, Shanghai, China).

Statistical Analysis

Results were expressed as mean ± SD. Statistical differences were evaluated using one-way ANOVA and *post hoc* tests using the SPSS statistical analysis software (version 14.0).

RESULTS

MAN Alleviated the Joints Destruction in CIA Rats

To achieve better therapeutic effects *in vivo*, the regimen was optimized based on previous studies [5, 6], and finally, the dose of 40 mg/kg/day was adopted. Significant signs of inflammation including swelling and redness in paws of CIA rats were observed throughout the experiments. During the later stage, soft tissue swelling was reduced, but significant ankylosis and deformation were developed in all the limbs. MAN intervention greatly eased inflammatory manifestation and improved motor functions in CIA rats (Fig. 1a). Radiological examinations showed that CIA rats suffered from severe joints architecture damages. Joint space narrowing, bone erosion, and bone density loss could be readily observed. All these pathological changes were ameliorated by MAN, while the most significant effect appeared to be the reduced ossifications especially in the interphalangeal regions (Fig. 1b). Histological examinations further validated the successful development of CIA in rats. The joints structures were extensively damaged in CIA rats. The cartilage and subchondral bone were severely eroded by the expanded synovium. Inflammatory infiltration and pannus formation also occurred (Fig. 1c). Likewise, MAN treatment efficiently inhibited synovial hyperplasia and matrix degradation.

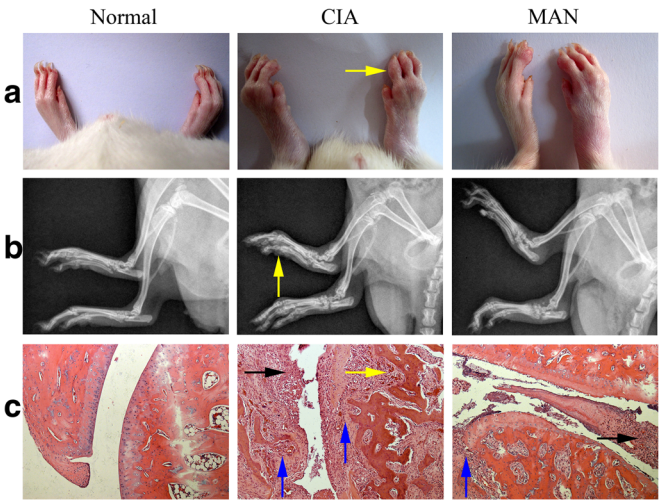

Fig. 1. Therapeutic effects of MAN on CIA in rats. **a**, morphological observation of hind paw (yellow arrow: bulbous swelling of proximal interphalangeal joints); **b**, radiography image of hind limb (yellow arrow: joint space narrowing and bone erosion); **c**, histological examination of ankle joints from hind paw (black arrow: synovial hyperplasia and inflammatory infiltration, yellow arrow: pannus formation, blue arrow: erosion of cartilage and bone).

MAN Treatment Compromised Nicotinamide Metabolism in CIA Rats

PCA revealed a separation tendency of metabolic profiling among rat groups, while the results from OPLS-DA further sharpened the separation (Supplementary S1). Those potential discriminatory variables sharing fragmentation patterns similarity over 60% with references in the library were identified, visualized in the heat-maps (Fig. 2a and Supplementary S2), and used for pathway enrichment analysis using KEGG database. Restored amino acids, ketone bodies, and thiamine metabolism balances in the CIA rats were revealed under MAN treatment (Fig. 2b and Supplementary S3), suggesting a substantial recovery from the high energy consumption and matrix degradation conditions. Additionally, pathway analysis under negative mode found MAN significantly altered nicotinate and nicotinamide metabolism (Fig. 2b). As NAD biosynthesis is critical for maintaining physiological and pathological functions, such changes would have profound effects *in vivo*. Hence, we further traced the changes of all relevant discriminatory metabolites (Supplementary S4), and found MAN significantly reduced levels of many important intermediates involved in NAD biosynthesis (Fig. 3a). Although its precursor nicotinamide (NAM) were barely affected, NMN was reduced by 67% upon MAN treatment (Fig. 3b), suggesting that MAN could selectively suppress the salvage, but not *de novo* biosynthesis pathway of NAD, by down-regulation and/or inhibition of nicotinamide phosphoribosyltransferase (NAMPT), the rate-limiting enzyme in the catalytic procedure.

MAN Reduced NAMPT Expression in Synovium and NAD^+ Production in Serum

To test the above hypothesis, we investigated the expression of NAMPT in synovium and the level of NAD^+ in serum. Expression of NAMPT in CIA rats was significantly increased compared to that in normal controls (Fig. 4A). Consistent with a previous report, we also noticed that strong NAMPT positive cells were mainly located in the synovial lining layer [7]. MAN treatment significantly reduced the expression of NAMPT (Fig. 4B). As expected, the decrease in NAMPT expression in synovium was accompanied with a decrease of NAD^+ in serum (Fig. 4C). These results strongly support our claim that MAN treatment decreases NAMPT expression and therefore compromises the salvage biosynthesis of NAD.

The Levels of NAMPT and NAD in HFLS-RA Cells Were Also Suppressed by MAN

To further investigate the effects of MAN on NAMPT expression and the consequent cellular changes, we performed additional *in vitro* studies in HFLS-RA cells. Preliminary studies demonstrated that the effects of MAN on NAMPT and NAD were highly dependent on treatment time. We suspected that this could be due to accumulation of dead cells upon prolonged exposure to MAN and therefore performed the MTT assay. We found that MAN at the concentration up to 12 μg/ml did not cause obvious cell death upon 6-h treatment (data not shown). Co-treatment

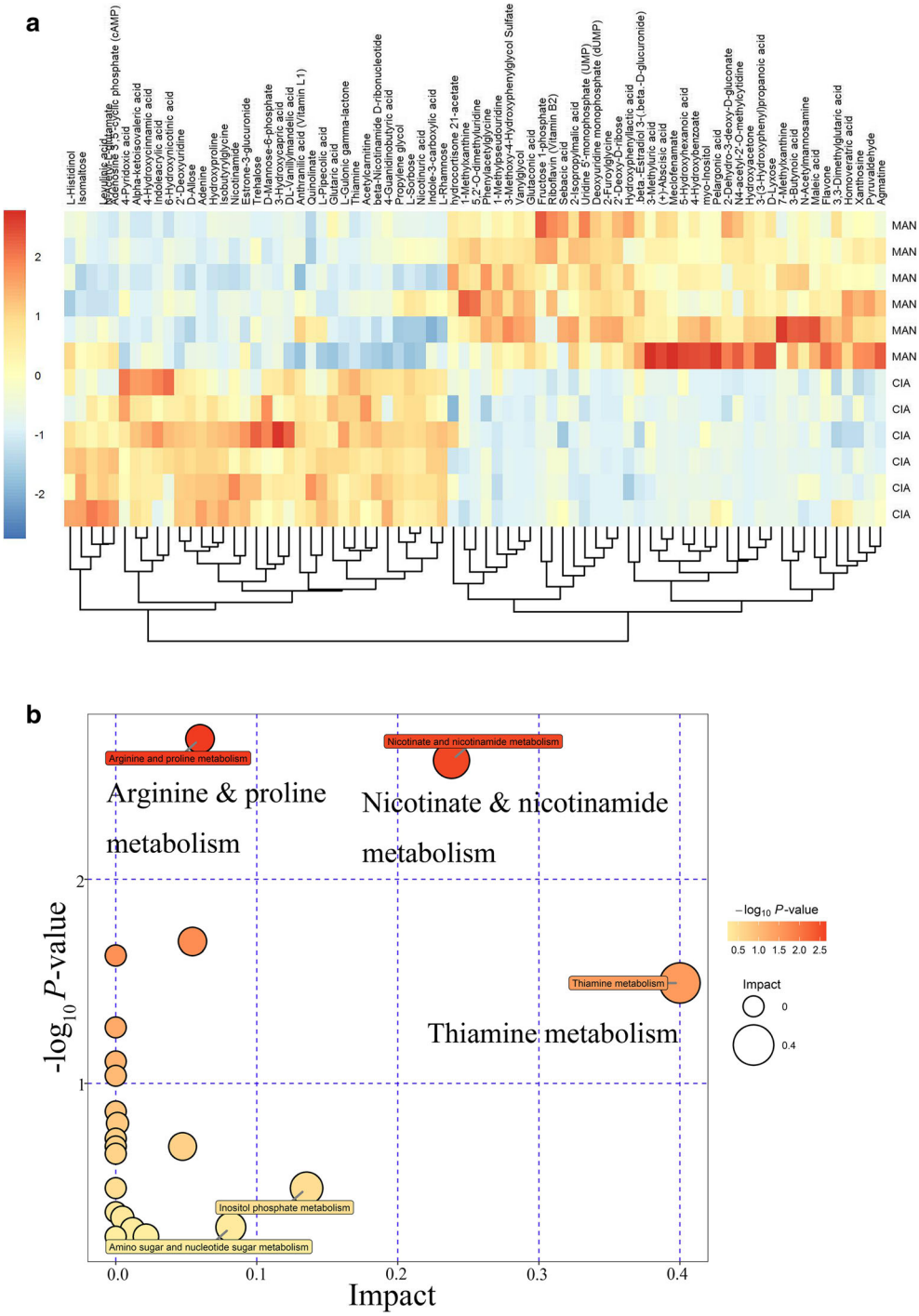

Fig. 2. Effects of MAN treatment on metabolic profile of CIA rats revealed by the UPLC-MS/MS analysis of urine samples. **a** Discriminating metabolites between MAN and CIA groups discovered under negative mode (VIP > 1, $p < 0.05$); **b** altered metabolic pathways in CIA rats by MAN treatment revealed under negative mode.

with NAD/NMN did not rescue cells from death, suggesting that crippled NAD biosynthesis had no or minor effects on cell viability (Fig. 5a). As apoptosis upon xanthone treatments was mainly driven by intracellular reactive oxygen species (ROS) accumulation [8], we evaluated oxidative stress in HFLS-RA cells potentially induced by

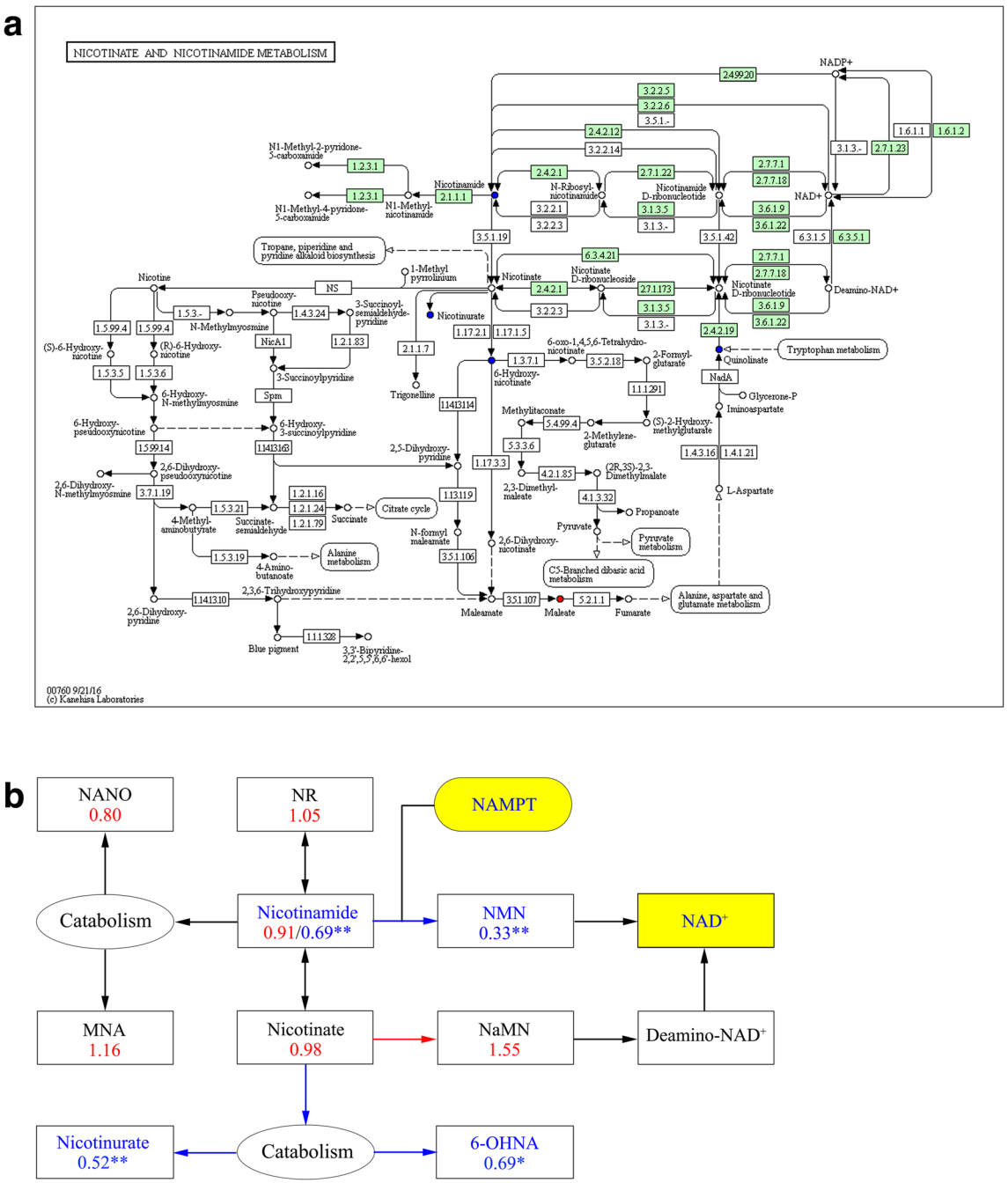

Fig. 3. Regulatory effects of MAN on nicotinate and nicotinamide metabolism in CIA rats. **a** Main intermediates from this metabolic pathway regulated by MAN treatment (data acquired from negative mode; blue, down-regulation, red, up-regulation); **b** possible effects of MAN on NAD biosynthesis indicated by intermediates changes; numbers indicate fold change compared with CIA models; colors of metabolites: blue, down-regulation; colors in numbers indicate acquisition sources of the data: blue, negative mode, red, positive mode; NR, 6-OHNA, NaMN, MHA, and NANO represented nicotinamide riboside, 6-hydroxynicotinic acid, nicotinate mononucleotide, 1-methylnicotinamide, and nicotinamide N-oxide, respectively.

MAN to further optimize treatments to minimize cytotoxicity. Consistent with results from the MTT assay, no obvious ROS accumulation was observed until 12 h after MAN treatment at 12 μg/ml (Fig. 5b).

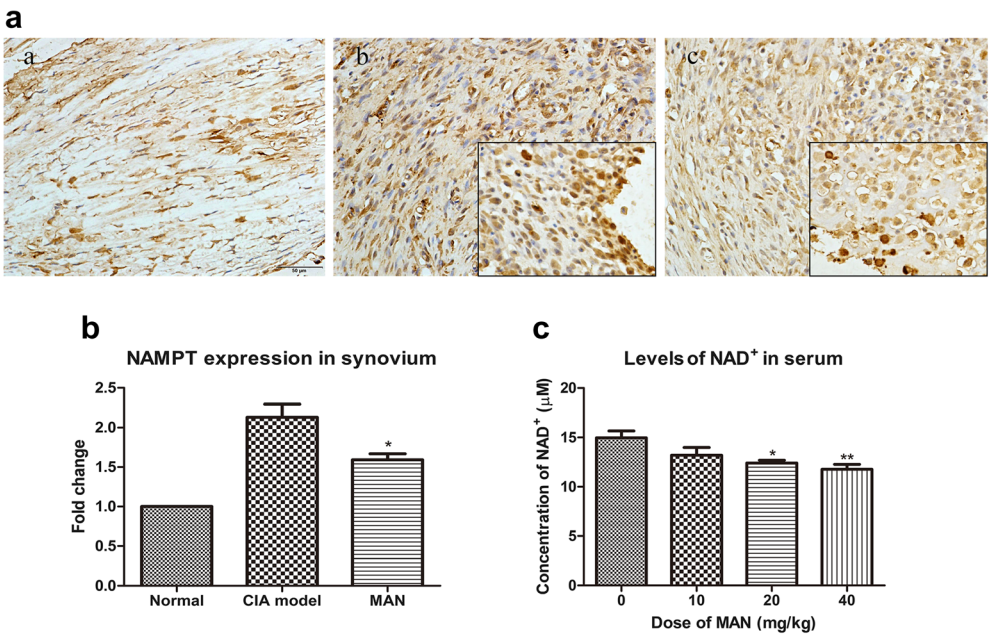

Fig. 4. Effects of MAN treatments on the levels of NAMPT and NAD *in vivo*. **a** NAMPT expression in synovium: a, normal; b, CIA model; c MAN treated; **b** quantitative result of A; **c** levels of NAD^+ in serum from rats receiving MAN treatment. Statistical significance: **b** $^{*}p < 0.05$ compared with CIA models; **c** $^{*}p < 0.05$ and $^{**}p < 0.01$ compared with untreated rats.

We further showed that MAN significantly affected NAD production in HFLS-RA cells in a time-dependent manner. Both NAD^+ and NADH were significantly decreased upon MAN treatment for 6 h. In contrast, their levels were significantly increased by 24-h treatment. The similar phenomenon also occurred on the intracellular NAD^+/NADH ratio, which was increased in a concentration-dependent manner upon 6-h treatment, but significantly decreased 18 h later (Fig. 5c).

These results imply that the effects of MAN on NAMPT are also possibly treatment time dependent. Subsequently, we investigated expression of NAMPT in HFLS-RA cells at different treatment time points. MAN decreased intracellular NAMPT (iNAMPT) expression within the first 6 h; however, the expression of iNAMPT was increased, rather than decreased, after 24-h treatment (Fig. 5d, e). MAN treatments resulted in similar but not exactly synchronous changes in the levels of extracellular NAMPT (eNAMPT). The most effective decrease in iNAMPT occurred at 3 h after MAN treatment, while the most pronounced effects of MAN on eNAMPT occurred at 6 h (Fig. 5f).

It appears that the inhibitory effect of MAN on iNAMPT expression was gradually diminished by the decrease in cell viability and completely turned to the opposite by the increase of apoptotic cells. The intracellular ROS elicited by MAN definitely should account for these changes *via* the well-established ROS-NAMPT feedback [9]. Meanwhile, extracellular NAD released from the apoptotic cells could also play a critical role in promoting iNAMPT expression in response to high oxidative stress, as extracellular NAD serves as an important rescue signal during apoptosis [10]. In consistent to this assumption, co-treatment with NAD significantly restored the MAN-induced decrease of iNAMPT in cells (Fig. 5g).

LPS treatment induced a significant increase of eNAMPT in HFLS-RA cells, which was quenched by MAN (12 μg/ml for 6 h). Co-treatments with NAD and NMN exhibited an overall antagonistic effect against MAN-induced decrease of eNAMPT (Fig. 5h). Despite of its strong positive effects on iNAMPT expression, NAD showed rather weak effects on eNAMPT secretion; however, supplement with NMN achieved a significant recovery. Extracellular NAD cannot permeate into cells, and it does not contribute much to the intracellular levels of NAD [11]. Unlikely, incubation with NMN, the main precursor for NAD in mammals, will directly augment the NAD production. Thus, our data suggest that, although the level of eNAMPT is closely correlated with iNAMPT, its fluctuation upon MAN treatment could be mainly driven by intracellular NAD.

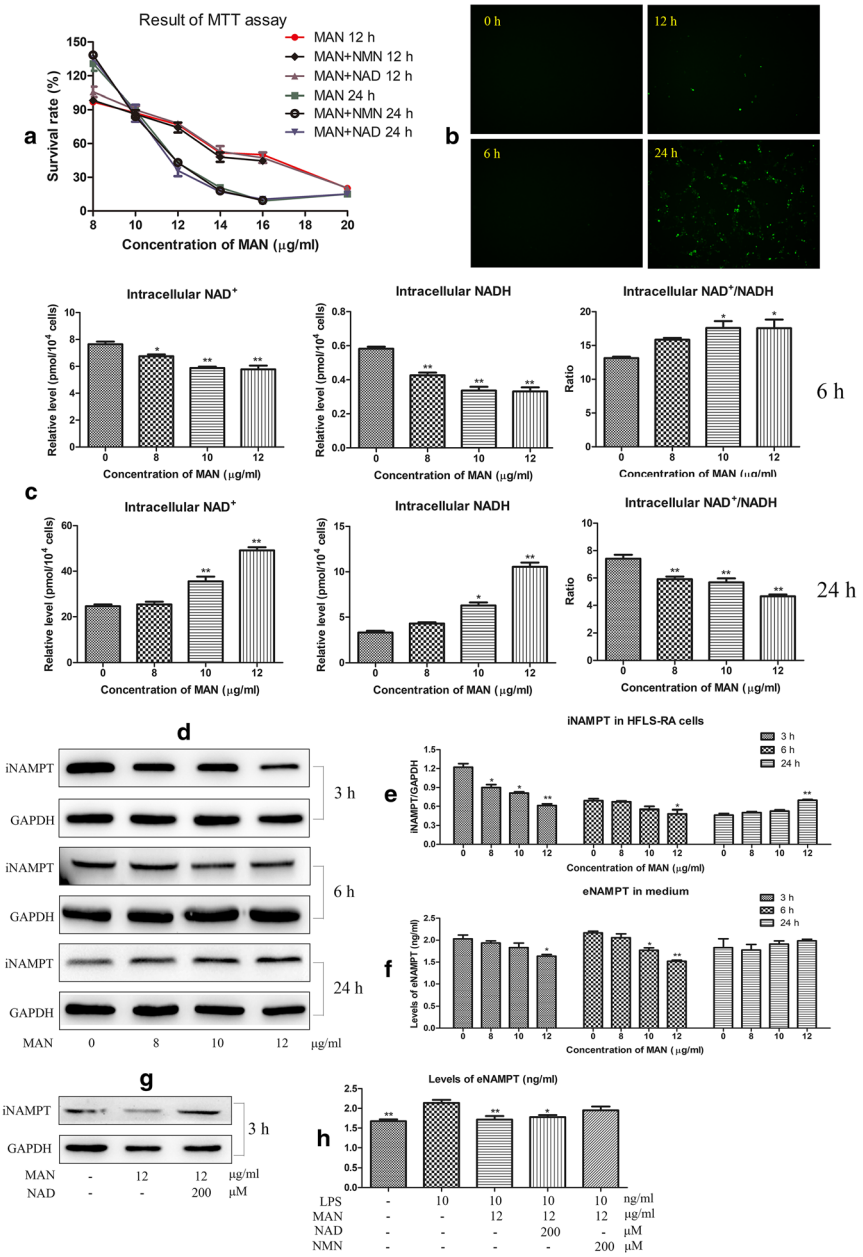

Fig. 5. Effects of MAN on the levels of NAMPT and NAD in HFLS-RA cells *in vitro*. **a** Survival rates of cells investigated by MTT assay; **b** MAN at 12 μg/ml elicited intracellular ROS accumulation in the time-dependent manner; **c** the relative levels of intracellular NAD^+/NADH; **d** expression of iNAMPT in HFLS-RA cells; **e** quantitative result of **d**; **f** secretion of eNAMPT by HFLS-RA cells; **g** expression of iNAMPT under the co-treatment with NAD and MAN; **h** secretion of eNAMPT under the co-treatments with NAD/NMN and MAN. Statistical significance: **c**–**f**, $^{*}p < 0.05$ and $^{**}p < 0.01$ compared with untreated cells; **h** $^{*}p < 0.05$ and $^{**}p < 0.01$ compared with LPS-treated cells.

MAN Treatment Reduced the Expression of Sirt1 in FLS both *in vivo* and *in vitro*

Sirt1, a NAD-consuming deacetylase, was highly expressed in both FLS and immune cells in the synovium from CIA rats compared with normal animals (Fig. 6A). Similar to effects on NAMPT, treatment with MAN led to a significant reduction of Sirt1 *in vivo* (Fig. 6B). *In vitro*, MAN treatments induced a remarkable decrease in Sirt1 expression in HFLS-RA cells initially in a dose-dependent manner; however, the effects gradually

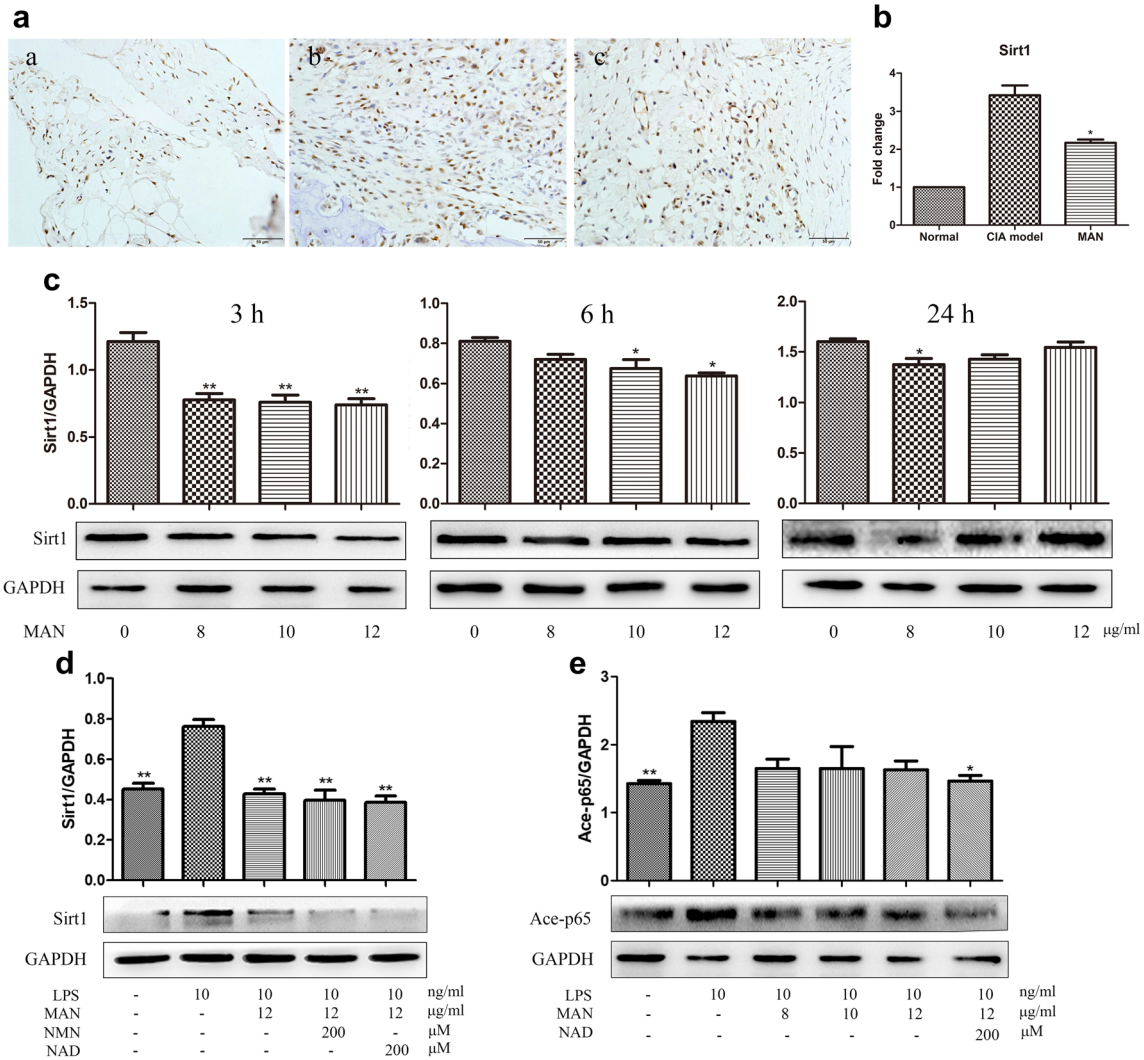

Fig. 6. Effects of MAN on the expression of Sirt1 and ace-p65 in FLS. **a** Expression of Sirt1 in synovium in rats: a, normal; b, CIA model; c MAN treated; **b** quantitative result of **a**; **c** expression of Sirt1 in HFLS-RA cells under MAN treatments; **d** expression of Sirt1 in HFLS-RA cells under the co-treatments of NAD/NMN and MAN for 6 h; **e** expression of ace-p65 in HFLS-RA cells under the co-treatments of NAD and MAN for 6 h. Statistical significance: **b** $^{*}p < 0.05$ compared with CIA models; **c** $^{*}p < 0.05$ and $^{**}p < 0.01$ compared with untreated cells; **d-e** $^{*}p < 0.05$ and $^{**}p < 0.01$ compared with LPS-treated cells.

diminished (Fig. 6C). Co-treatments with either NAD or NMN just showed slight synergistic effects on MAN-mediated down-regulation of Sirt1 in LPS-treated HFLS-RA cells (Fig. 6D), which suggested that regulation of Sirt1 by MAN is not highly dependent on changes in NAMPT/NAD.

For Sirt1 deacetylates the p65 subunit of NF-κB, down-regulation of Sirt1 would cause ace-p65 accumulation theoretically [12]. However, the levels of ace-p65 were not increased, but rather decreased to some extent after MAN treatments for 6 h. Co-treatments with NAD and MAN further reduced ace-p65, indicating that the increase in NAD is favorable for deacetylation of p65 (Fig. 6E).

Inhibition of NAMPT/NAD by MAN Led to Reduced Inflammations

Considering the well-established relationship between NAMPT controlled energy expenditure and inflammation reactions [13], we assumed that the alleviation of NF-κB-mediated inflammation by MAN could be linked to inhibition of NAMPT-related signal transductions. It

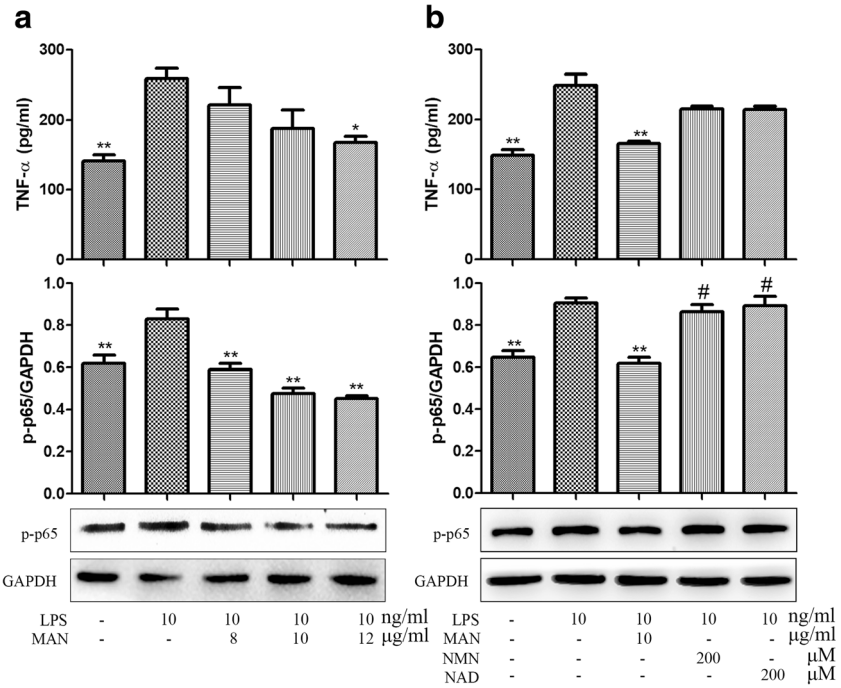

Fig. 7. Effects of MAN on the levels of p-p65 and TNF-α in HFLS-RA cells *in vitro*. **a** Inhibitory effects of MAN treatments (for 6 h) on increased levels of p-p65 and TNF-α induced by LPS stimulus; **b** levels of p-p65 and TNF-α under the co-treatments of NAD/NMN and MAN (for 6 h). Statistical significance: $^{*}p < 0.05$ and $^{**}p < 0.01$ compared with LPS-treated cells; $^{\#}p < 0.05$ compared with LPS + MAN-treated cells.

was found that MAN treatments for 6 h efficiently suppressed the increase of p-p65 in HFLS-RA cells induced by LPS in a concentration-dependent manner. This decrease consequently led to declined secretion of TNF-α (Fig. 7a). These changes were then significantly reverted by either NAD or NMN co-incubations (Fig. 7b). The results suggest that the down-regulation of NAMPT/NAD by MAN profoundly inhibited the hyper-activation of NF-κB and subsequent secretion of pro-inflammatory cytokines.

DISCUSSION

Conceptualization of the feedback in energy metabolism and inflammation provides us with a novel perspective to think about the pathogenesis and therapeutic strategy of some chronic diseases [13]. As well recognized, intensive energy consuming molecular events are involved in inflammation reactions. Logically, reducing in energy supply could likely curb the persistence of inflammations, which has been solidly supported by the calorie restriction regimen [14]. Hence, intervention in the energy metabolism could be a reasonable strategy in therapies of complicated inflammatory diseases, such as RA.

NAM is the predominant precursor for NAD biosynthesis in mammals. By converting NAM into NMN, NAMPT plays a decisive role in the NAD production in the salvage pathway, and subsequently controls energy homeostasis. However, increasing reports suggest that over-expression of NAMPT is implicated in the development of tumors and inflammations [11]. In the specific case of RA, NAMPT, especially the extracellular form, is significantly increased, and its level is positively correlated with radiographic joints damages [15]. Hence, it is reasonable to hypothesize that inhibition of NAMPT by MAN plays a crucial role in therapeutic actions on CIA.

Results from this study explicitly revealed the therapeutic effects of MAN on CIA in rats and their relevance to down-regulated expression of NAMPT in FLS. We also partially elucidated the underlying molecular mechanisms. Busso et al. reported that the specific inhibitor of NAMPT, APO886, reduced the severity of CIA in mice. They believed that the anti-inflammatory property of APO886 was mainly due to its inhibition on the enzymatic activity of NAMPT [16]. Similarly, we showed that MAN treatments down-regulated NAMPT expression both *in vitro* and *in vivo*, which was accompanied with reduced NAD production, NF-κB activation, and TNF-α secretion. Furthermore, inhibition of NF-κB activation and TNF-α secretion

by MAN was reverted by co-treatment with NMN. It strongly suggests that manipulation of NAD production is crucial for therapeutic effects of MAN on CIA. It also raised a question: why reduction in NAD production could ease the inflammation reactions in CIA rats?

It is eNAMPT, but not iNAMPT, who mainly perpetuates inflammations under pathological conditions [7] by functioning as a pro-inflammatory cytokine [16]. Strikingly, it can directly bind to TLR4 and stimulate robust activation of NF-κB pathway [17]. Therefore, we presume that MAN-mediated reduction of eNAMPT could be the main factor accounting for the therapeutic effects on CIA. Because eNAMPT is produced through post-translational modification from iNAMPT, the decrease of iNAMPT induced by MAN would eventually lead to the reduction of eNAMPT (Fig. 5e, f). More importantly, eNAMPT is the product from the deacetylation of iNAMPT catalyzed by Sirt1 [18], indicating that the production of eNAMPT is a highly NAD consuming procedure which will be substantially limited under the shortage of NAD supply. This notion was also testified. Co-treatment of MAN with NMN significantly restored the decrease in eNAMPT brought about by MAN in cells (Fig. 5h). Thus, we suggest that, albeit reduction of eNAMPT possesses more direct influences on therapeutic outcomes of MAN on CIA, down-regulation of iNAMPT is similarly important. Not only does it provide the precursor, iNAMPT also fuels the secretion of eNAMPT by promoting NAD synthesis. The lagged decrease of eNAMPT came after the regulation of iNAMPT by MAN (Fig. 5e, f) further supports our conclusion.

Sirt1 is a key metabolic sensor that modulates mammalian metabolic homeostasis in response to various signals [19]. Theoretically, fluctuation of NAMPT/NAD will inevitably affect Sirt1. Despite anti-inflammatory effects of Sirt1 are well recognized, its role in RA remains controversial. Some studies suggest that Sirt1 activation is beneficial in treatments of RA *via* deacetylation of p65 and subsequent inhibition of NF-κB pathway [20]. However, increasing evidences suggest that over-expression of Sirt1 in synovium is a common characteristic of RA, which is implicated in over production of pro-inflammatory cytokines and apoptosis resistance of FLS [21]. Therefore, targeting Sirt1 would suppress overall inflammatory activation and achieve notable therapeutic efficacy [22]. Although we showed that MAN significantly reduced Sirt1 expression both *in vivo* and *in vitro*, its clinical implication is not clear without fundamental mechanistic understanding. We thought reduced expression of Sirt1 would result in accumulation of ace-p65 and thus pose a negative impact on inflammation. On the contrary, the levels of ace-p65 were decreased upon MAN treatment (Fig. 6E). A previous study provides us some clues to solve this puzzle. Apart from the absolute levels of NAD, the NAD^+/NADH ratio also plays a critical role in balancing Sirt1 activity [23]. Hence, the decrease in ace-p65 elicited by MAN could possibly be the result from increased NAD^+/NADH ratio.

FUNDING

This work was supported by the National Natural Science Foundation of China (81603388), Research Project on Traditional Chinese medicine of Anhui province (2016zy37), Key Project of Natural Science Foundation of Anhui Province for College Scholar (KJ2018A0249), and Project of Construction on Key Discipline of State Administration of Traditional Chinese Medicine (2012-32).

COMPLIANCE WITH ETHICAL STANDARDS

Conflict of Interest. The authors declare that they have no conflict of interest.

Ethical Approval. The animal experimental protocols were approved by Ethical Committee of Yijishan Hospital and strictly in accordance with the guideline for the care and use of laboratory animals (US National Research Council, 2011).

REFERENCES

1. Zuo, J., K.J. Mao, F. Yuan, X. Li, and J.W. Chen. 2014. Xanthones with anti-tumor activity isolated from *Securidaca inappendiculata*. *Medicinal Chemistry Research* 23: 4865–4871.
2. Zuo, J., Y. Xia, X. Li, and J.W. Chen. 2014. Xanthones from *Securidaca inappendiculata* exert significant therapeutic efficacy on adjuvant-induced arthritis in mice. *Inflammation* 37: 908–916.
3. Zuo, J., Y. Xia, X. Li, Z. Ou-Yang, and J.W. Chen. 2015. Selective modulation of MAPKs contribute to the anti-proliferative and anti-inflammatory activities of 1,7-dihydroxy-3,4-dimethoxyxanthone in rheumatoid arthritis-derived fibroblast-like synoviocyte MH7A cells. *Journal of Ethnopharmacology* 168: 248–254.
4. Pedraza-Chaverri, J., N. Cardenas-Rodriguez, M. Orozco-Ibarra, and J.M. Perez-Rojas. 2008. Medicinal properties of mangosteen (*Garcinia mangostana*). *Food & Chemmical Toxicology* 46: 3227–3239.
5. Zuo, J., Q. Yin, Y.W. Wang, Y. Li, L.M. Lu, Z.G. Xiao, G.D. Wang, and J.J. Luan. 2018. Inhibition of NF-κB pathway in fibroblast-like synoviocytes by α-mangostin implicated in protective effects on

joints in rats suffering from adjuvant-induced arthritis. *International Immunopharmacology* 56: 78–89.
6. Zuo, J., Q. Yin, L. Wang, W. Zhang, Y. Fan, Y.Y. Zhou, Y. Li, and G.D. Wang. 2018. Ethanol extract of mangosteen alleviated the severity of collagen-induced arthritis in rats and produced synergistic effects with methotrexate. *Pharmaceutical Biology*. https://doi.org/10.1080/13880209.2018.1506939 In press.
7. Brentano, F., O. Schorr, C. Ospelt, J. Stanczyk, R.E. Gay, S. Gay, and K. Diego. 2010. Pre-B cell colony-enhancing factor/visfatin, a new marker of inflammation in rheumatoid arthritis with proinflammatory and matrix-degrading activities. *Arthritis and Rheumatism* 56: 2829–2839.
8. Zuo, J., D.Y. Dou, H.F. Wang, Y.H. Zhu, Y. Li, and J.J. Luan. 2017. Reactive oxygen species mediated NF-κB/p38 feedback loop implicated in proliferation inhibition of HFLS-RA cells induced by 1,7-dihydroxy-3,4-dimethoxyxanthone. *Biomedicine & Pharmacotherapy* 94: 1002–1009.
9. Wang, B., M.K. Hasan, E. Alvarado, H. Yuan, H. Wu, and W.Y. Chen. 2011. Nampt overexpression in prostate cancer and its contribution to tumor cell survival and stress response. *Oncogene* 30: 907–921.
10. Pliyev, B.K., A.V. Ivanova, and V.G. Savchenko. 2014. Extracellular NAD^+ inhibits human neutrophil apoptosis. *Apoptosis* 19: 581–593.
11. Garten, A., S. Schuster, M. Penke, T. Gorski, T.D. Giorgis, and W. Kiess. 2015. Physiological and pathophysiological roles of NAMPT and NAD metabolism. *Nature Reviews Endocrinology* 11: 535–546.
12. Kauppinen, A., T. Suuronen, J. Ojala, K. Kaarniranta, and A. Salminen. 2013. Antagonistic crosstalk between NF-κB and SIRT1 in the regulation of inflammation and metabolic disorders. *Cellular Signalling* 25: 1939–1948.
13. Liu, T.F., C. Brown, M.E. Gazzar, L. McPhail, P. Millet, A. Rao, V.T. Vachharajani, B.K. Yoza, and C.E. McCall. 2012. Fueling the flame: Bioenergy couples metabolism and inflammation. *Journal of Leukocyte Biology* 92: 499–507.
14. Ye, J., and J.N. Keller. 2010. Regulation of energy metabolism by inflammation: A feedback response, in obesity and calorie restriction. *Aging* 2: 361–368.
15. Rho, Y.H., J. Solus, T. Sokka, A. Oeser, C.P. Chung, T. Gebretsadik, A. Shintani, T. Pincus, and C.M. Stein. 2014. Adipocytokines are associated with radiographic joint damage in rheumatoid arthritis. *Arthritis and Rheumatism* 60: 1906–1914.
16. Busso, N., M. Karababa, M. Nobile, A. Rolaz, F.V. Gool, M. Galli, O. Leo, A. So, and T.D. Smedt. 2008. Pharmacological inhibition of nicotinamide phosphoribosyltransferase/visfatin enzymatic activity identifies a new inflammatory pathway linked to NAD. *PLoS One* 3: e2267.
17. Camp, S.M., E. Ceco, C.L. Evenoski, S.M. Danilov, T. Zhou, E.T. Chiang, L. Moreno-Vinasco, B. Mapes, J. Zhao, G. Gursoy, M.E. Brown, D.M. Adyshev, S.S. Siddiqui, H. Quijada, S. Sammani, E. Letsiou, L. Saadat, M. Yousef, T. Wang, J. Liang, and J.G.N. Garcia. 2015. Unique toll-like receptor 4 activation by NAMPT/PBEF induces NFκB signaling and inflammatory lung injury. *Scientific Reports* 5: 13135.
18. Yoon, M.J., M. Yoshida, S. Johnson, A. Takikawa, I. Usui, K. Tobe, T. Nakagawa, J. Yoshino, and S. Imai. 2015. Sirt1-mediated eNAMPT secretion from adipose tissue regulates hypothalamic NAD^+ and function in mice. *Cell Metabolism* 21: 706–717.
19. Gallí, M., F. Van Gool, and O. Leo. 2011. Sirtuins and inflammation: Friends or foes? *Biomedicine & Pharmacotherapy* 81: 569–576.
20. Hah, Y.S., Y.H. Cheon, H.S. Lim, H.Y. Cho, B.H. Park, S.O. Ka, Y.R. Lee, D.W. Jeong, H.O. Kim, M.K. Han, and S.I. Lee. 2014. Myeloid deletion of SIRT1 aggravates serum transfer arthritis in mice via nuclear factor-κb activation. *PLoS One* 9: e87733.
21. Niederer, F., C. Ospelt, F. Brentano, M.O. Hottiger, R.E. Gay, S. Gay, M. Detmar, and D. Kyburz. 2011. Sirt1 overexpression in the rheumatoid arthritis synovium contributes to proinflammatory cytokine production and apoptosis resistance. *Annals of the Rheumatic Diseases* 70: 1866–1873.
22. Grabiec, A.M., S. Krausz, W.D. Jager, T. Burakowski, D. Groot, M.E. Sanders, B.J. Prakken, W. Maslinski, E. Eldering, P.P. Tak, and K.A. Reedquist. 2010. Histone deacetylase inhibitors suppress inflammatory activation of rheumatoid arthritis patient synovial macrophages and tissue. *Journal of Immunology* 184: 2718–2728.
23. Cantó, C., Z. Gerharthines, J.N. Feige, M. Lagouge, L. Noriega, J.C. Milne, P.J. Elliott, P. Puigserver, and J. Auwerx. 2009. Ampk regulates energy expenditure by modulating NAD^+ metabolism and SIRT1 activity. *Nature* 458: 1056–1060.